



HAL
open science

Solving Controversies on the Iron Phase Diagram Under High Pressure

Guillaume Morard, Silvia Boccato, Angelika D Rosa, Simone Anzellini, Francesca Miozzi, Laura Henry, Gaston Garbarino, Mohamed Mezouar, Marion Harmand, François Guyot, et al.

► **To cite this version:**

Guillaume Morard, Silvia Boccato, Angelika D Rosa, Simone Anzellini, Francesca Miozzi, et al.. Solving Controversies on the Iron Phase Diagram Under High Pressure. *Geophysical Research Letters*, In press, 10.1029/2018GL079950 . hal-01924967

HAL Id: hal-01924967

<https://hal.science/hal-01924967>

Submitted on 16 Nov 2018

HAL is a multi-disciplinary open access archive for the deposit and dissemination of scientific research documents, whether they are published or not. The documents may come from teaching and research institutions in France or abroad, or from public or private research centers.

L'archive ouverte pluridisciplinaire **HAL**, est destinée au dépôt et à la diffusion de documents scientifiques de niveau recherche, publiés ou non, émanant des établissements d'enseignement et de recherche français ou étrangers, des laboratoires publics ou privés.

Solving controversies on the iron phase diagram under high pressure

**Guillaume MORARD,^{1*} Silvia BOCCATO,² Angelika D. ROSA,² Simone ANZELLINI,³
Francesca MIOZZI,¹ Laura HENRY,² Gaston GARBARINO,² Mohamed MEZOUAR,²
Marion HARMAND,¹ François GUYOT,¹ Eglantine BOULARD,¹ Innokenty KANTOR,^{2,4}
Tetsuo IRIFUNE,⁵ Raffaella TORCHIO²**

¹Sorbonne Université, Institut de Minéralogie, de Physique des Matériaux et de Cosmochimie, IMPMC, Museum National d'Histoire Naturelle, UMR CNRS 7590, IRD, 4 Place Jussieu, 75005 Paris, France.

²European Synchrotron Radiation Facility, Grenoble, France

³Diamond Light Source Ltd., Diamond House, Harwell Science Campus, Didcot, OX11 0DE, UK

⁴Danmarks Tekniske Universitet, Institut for Fysik, Kgs. Lyngby, 2800, DK

⁵GRC, Ehime University, Japan

Corresponding author: Guillaume Morard (guillaume.morard@upmc.fr)

Key Points:

- Melting curve and phase diagram of pure Fe has been measured by in situ X-ray absorption up to 130 GPa
- Overall agreement between different in situ studies leads to a melting temperature of 4250 ± 250 K at Core Mantle Boundary pressure.
- Discrepancies with previous measurements is unambiguously attributed to carbon contamination from the diamonds or thermal pressure overestimation

Abstract

As the main constituent of planetary cores, pure iron phase diagram under high pressure and temperature is of fundamental importance in geophysics and planetary science. However, previously reported iron melting curves show large discrepancies (up to 1000 K at the Earth's core-mantle boundary (136 GPa)), resulting in persisting high uncertainties on the solid-liquid phase boundary. Here we unambiguously show that the observed differences commonly attributed to the nature of the used melting diagnostic are due to a carbon contamination of the sample as well as pressure overestimation at high temperature. The high melting temperature of pure iron under core-mantle boundary (4250 ± 250 K), here determined by X-ray absorption experiments at the Fe K-edge, indicates that volatile light elements such as sulfur, carbon or hydrogen are required to lower the crystallization temperature of the Earth's liquid outer core in order to prevent extended melting of the surrounding silicate mantle.

Plain language summary

Iron is the main constituent of planetary cores, however there are still large controversies regarding its melting temperature and phase diagram under planetary interiors conditions. The present study reconciles different experimental approaches using Laser-Heated Diamond Anvil Cell with different in situ X-ray diagnostics (absorption, diffraction and Mossbauer spectroscopy). The main reason of discrepancies (over 1000 K at Core-Mantle Boundary (CMB) conditions) is attributed to carbon contamination from the diamond anvils, and metrology issues related to thermal pressure overestimation. A high melting temperature for iron at CMB pressure would imply the presence of volatiles elements in the liquid outer core, such as sulfur, carbon or hydrogen, in order to lower its crystallization temperature and avoid extended melting of the surrounding silicate mantle.

1 Introduction

Iron represents the main constituent of planetary cores in our solar system. Its physical properties under high pressure and temperature conditions are therefore extremely important to determine the internal structure and dynamics of telluric planets. One of the key parameters of its phase diagram is the melting curve. Its extrapolation up to the inner-outer core boundary (IOCB)

conditions can, in fact, provide information about the temperature profile in planetary cores. This information places important constraints on parameters like heat flux to the mantle, convectional mode and cooling rate, all of which are fundamental to the planets heat budget and dynamics. However, despite intensive experimental and theoretical efforts, a consensus on the melting line of pure iron has not been found during the last decades.

Pioneering work performed in laser-heated diamond anvil cells (LH-DAC) was using laser speckle technique to detect movement on the sample surface as melting diagnostic [Boehler, 1993]. This study has been later confirmed by an *in-situ* LH-DAC XRD study using the appearance of diffuse scattering as melting criterion [Boehler *et al.*, 2008] and recently confirmed again by *in-situ* X-ray absorption technique in LH-DAC [Aquilanti *et al.*, 2015]. Another recent *in-situ* LH-DAC XRD experiment, also using the appearance of diffuse scattering as melting criterion [Anzellini *et al.*, 2013] has obtained a melting line higher by more than 1000 K above 100 GPa with respect to the XAS measurement [Aquilanti *et al.*, 2015], but in a good agreement with shock experiments [Brown and McQueen, 1986; Nguyen and Holmes, 2004] and ab initio calculations [Alfè *et al.*, 2002; Alfè, 2009]. Finally, recent LH-DAC Synchrotron Mossbauer Spectroscopy (SMS) experiments [Jackson *et al.*, 2013; Zhang *et al.*, 2015] have determined a melting temperature falling in between the two previous curves.

The persisting discrepancies in the reported results have caused a longstanding debate among the scientists in the last years, in particular while comparing the adopted *in-situ* techniques. In fact, even if probing the sample under different scales of resolution of the atomic arrangement (XAS, SMS, XRD), these techniques should provide the same results within the experimental errors. However, while performing a LH-DAC experiment, several aspects must be considered together with the melting diagnostic to obtain reliable data, which include the sample configuration, possible chemical reactions and the adopted metrology (see Mezouar *et al.*, 2017). Furthermore, an accurate pressure and temperature evaluation at simultaneous high P/T conditions together with a critical assessment of their errors is essential to provide a reliable measure of the melting line.

In the present study, with the purpose of performing a critical comparison between different melting diagnostics, the melting line of pure Fe has been investigated *in situ* in LH-DAC by energy dispersed XAS. This is a probe similar to the one employed in [Aquilanti *et al.*, 2015]. The sample geometry of this study is identical to the one adopted in [Jackson *et al.*, 2013]

and in [Anzellini *et al.*, 2013], but strongly different than the one used in [Aquilanti *et al.*, 2015] (where the iron sample is contained a cavity drilled by FIB technique in Al_2O_3 single crystals). In addition, a critical analysis of the metrology has been performed during the experiment in order to establish realistic error bars. Finally, an *ex situ* analysis of the recovered samples has been performed by XRD and SEM techniques to evaluate the presence of chemical reactions and to validate the adopted melting criterion.

The obtained results reveal the different origins of discrepancies between previous studies therefore placing higher constrains on the iron melting line. We show that low melting line is related to carbon contamination and difference in the pressure determination at high temperature. Moreover, the present study provides a refined iron phase diagram up to Core-Mantle Boundary (CMB) pressure, allowing a better evaluation of the amount of light elements present in the core.

2 Materials and Methods

2.1 Experimental procedure

Laser-Heating Diamond Anvil Cell experiments were performed on the dispersive X-ray absorption beamline ID24 at the ESRF, Grenoble [Pascarelli *et al.*, 2016]. A highly focused X-ray beam was employed (down to $3 \times 3 \mu\text{m}^2$ FWHM) covering an energy range of more than 800 eV (i.e, from 7000-7800 eV). Two YAG lasers are focused on the sample using two separate plano-convex lenses with a focal distance of 50 mm, to obtain a laser hot-spot on the sample of 15-20 μm of diameter. Detailed description of the laser-heating experimental set-up available on ID24 beamline is detailed in [Kantor *et al.*, 2018].

Membrane driven LeToullec type diamond anvil cells were used to pressurize the sample equipped with either single crystal or sintered nano-polycrystalline diamonds [Ishimatsu *et al.*, 2012], having culet sizes ranging from flat 300 to beveled 300/150 μm . The latter allowed acquiring glitch-free XAS data over the entire energy range accessible at ID24. The sample consist of a 5 μm thick Fe foil (99.99% purity, GoodFellow), providing an optimized absorption jump. The employment of such thin samples further minimizes axial temperature gradients during laser heating. For all experiments, the Fe foil was sandwiched between two disks of KCl. These disks were prepared by compressing KCl powder to the target thickness (Sigma Aldrich, 99.99% purity). Single-disks were then laser-cut using the femto-laser micro machining facility available at IMPMC laboratory. The employment of pre-compressed KCl disks ensures a

controlled and homogeneous insulation thickness, which is a pre-requisite for generating a homogenous laser-heating spot reducing the temperature gradients seen by the X-rays. The disks further allowed performing reproducible and fast loadings. In order to limit and remove any contamination of moisture from air, the loading of the pressure medium and the sample were performed within maximal one hour and the loaded DAC was kept open in a vacuum oven at 120°C for more than 12 hours before pressurizing.

The temperature on the sample was gradually increased by adjusting the laser output power carefully stepwise every 0.1%. The temperature was measured with 1 to 0.01 second exposure time. The typical laser heating duration is 1.2 second, with a delay of 100 ms before starting the temperature measurement. XAS data were simultaneously acquired by accumulating 10 spectra with 100 ms exposure time. After each temperature step, a spectrum of the quenched sample was acquired to verify that the sample did not react. Details about the data acquisition procedure can be found in [Boccatto *et al.*, 2017].

The absence of reaction products such as Fe₃C was verified in all recovered samples by acquiring finely meshed (5 μm step size) 2D XRD maps at the diffraction beamline ID27 using a highly focused X-ray beam of 3x3 μm² ($\lambda=0.3738$ Å) [Mezouar *et al.*, 2005]. Diffraction images were integrated with Dioptas [Prescher and Prakapenka, 2015]. The Fe₃C phase could be identify in few samples through the presence of single diffraction spots of the most intense peaks of Fe₃C, i.e., (102) at 2.068 Å.

Recovered samples were cut through the hotspot area to analyze the texture using the analysis platform available at IMPMC. The developed technique combines femtosecond pulsed laser machining, ion polishing and FIB cutting, to remove the sample from the gasket and expose the laser-heated area, in order to perform accurate SEM imaging. Extended description of sample preparation can be found in [Morard *et al.*, 2017].

2.2 Thermal pressure calculation:

The pressure was determined at room temperature before and after each heating cycle using either the Raman peak position of the single-crystalline diamond measured at the center of the culet [Akahama and Kawamura, 2004] or using the position of the fluorescence line of a ruby sphere placed in the sample chamber [Dewaele *et al.*, 2008]. The sample pressure during laser-

heating was then calculated following the procedure established in Lord et al. (2015) and the equation:

$$P = P_{before} + \frac{P_{after} + \Delta P - P_{before}}{T_{max} - 300} * (T - 300)$$

Where P_{before} and P_{after} are the different pressures measured before and after the heating cycle, T_{max} is the maximal temperature of the heating cycle and ΔP is the pressure difference between the pressure at high temperature and the pressure measured after the heating cycle. This pressure difference is kept constant for the pressure-temperature range investigated in the present study and fixed at 2 GPa, as highlighted in a recent XRD experiment [Miozzi et al., 2018] (see Supplementary Materials and references therein for more details [Campbell et al., 2009; Lord et al., 2014]). It should be noticed that this equation is only valid for T_{max} superior to 2000 K, as the observed scattering of ΔP (2 ± 1.5 GPa, Figure S4) does not allow us assigning a dependence of ΔP over pressure or temperature.

3. Results

Solid-solid and solid-liquid phase transitions in iron can be unambiguously identified from changes in the XANES region of the absorption spectra at the Fe K-edge [Marini et al., 2014; Harmand et al., 2015; Torchio et al., 2016]. In particular, the transition from the high pressure hcp structure to the high temperature fcc structure results in a strong modification of the first XANES oscillation and the appearance of a double feature at 7130 and 7140 eV (Figure 1). Similarly, the solid to liquid transition results in marked changes of several XANES features: 1) in the pre-edge regions the shoulder at 7120 eV disappears and 2) the first XANES oscillation flattens. On this last point, it should be noticed that damping of these features related to melting is different from temperature damping of EXAFS oscillations due to Debye-Waller effect. The K-edge XANES of iron mirrors the electronic transition from the 1s to the empty 4p states. The observed smoothening of the XANES features in the liquid phase can be related to a broader distribution of empty 4p states due to the breaking of crystalline long-range order [Mazevet et al., 2014].

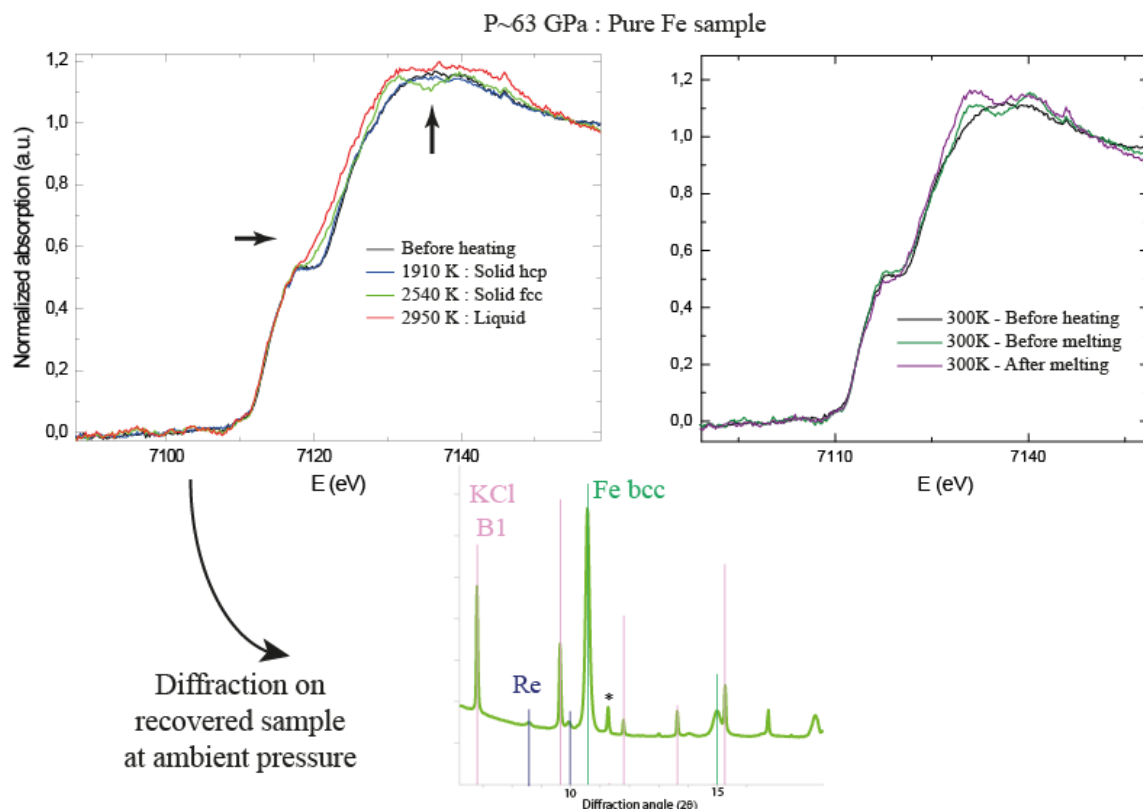


Figure 1: Evolution of XANES spectra at Fe absorption edge upon melting. Evolution of XANES spectra from hcp structure (in blue), to fcc structure (in green) and above the melting point (in red). Changes related to fcc-hcp transition are visible in the edge, with a change from one to two features in the edge. Changes related to melting is visible with the disappearance of the feature in the pre-edge and the flattening in the edge. Arrows indicate these modifications on the XANES signal. Corresponding spectra of quenched sample after each temperature do not show any change in the flank, in agreement with the absence of sample contamination. Diffraction spectrum of recovered sample indicates no additional phases, except one peak potentially belonging to the gasket holder (signaled by a star).

In order to confirm the validity of these *in situ* X-ray diagnostics, analysis of recovered samples were performed using a Focused Ion Beam (FIB) (Figure 2). The protocol for studying the recovered samples has been detailed in our previous work on iron alloys [Morard *et al.*, 2017]. Borders of the solid and the molten portions of the recovered samples exhibit a regular and an irregular shape respectively, allowing to discriminate between them. In addition, the texture related with solid grains twinning is visible in the solid portion of the sample, whereas the liquid portion is found to be homogeneous (central portion of the sample on Figure 2 and Figure S5). Thanks to these *ex situ* analyses we were able to validate the use of the disappearance of the features in the first oscillation and the flattening of the pre-edge in the XAS spectra, as

melting criteria for Fe, similar to our conclusions for the melting of Ni under high pressure [Boccatto *et al.*, 2017].

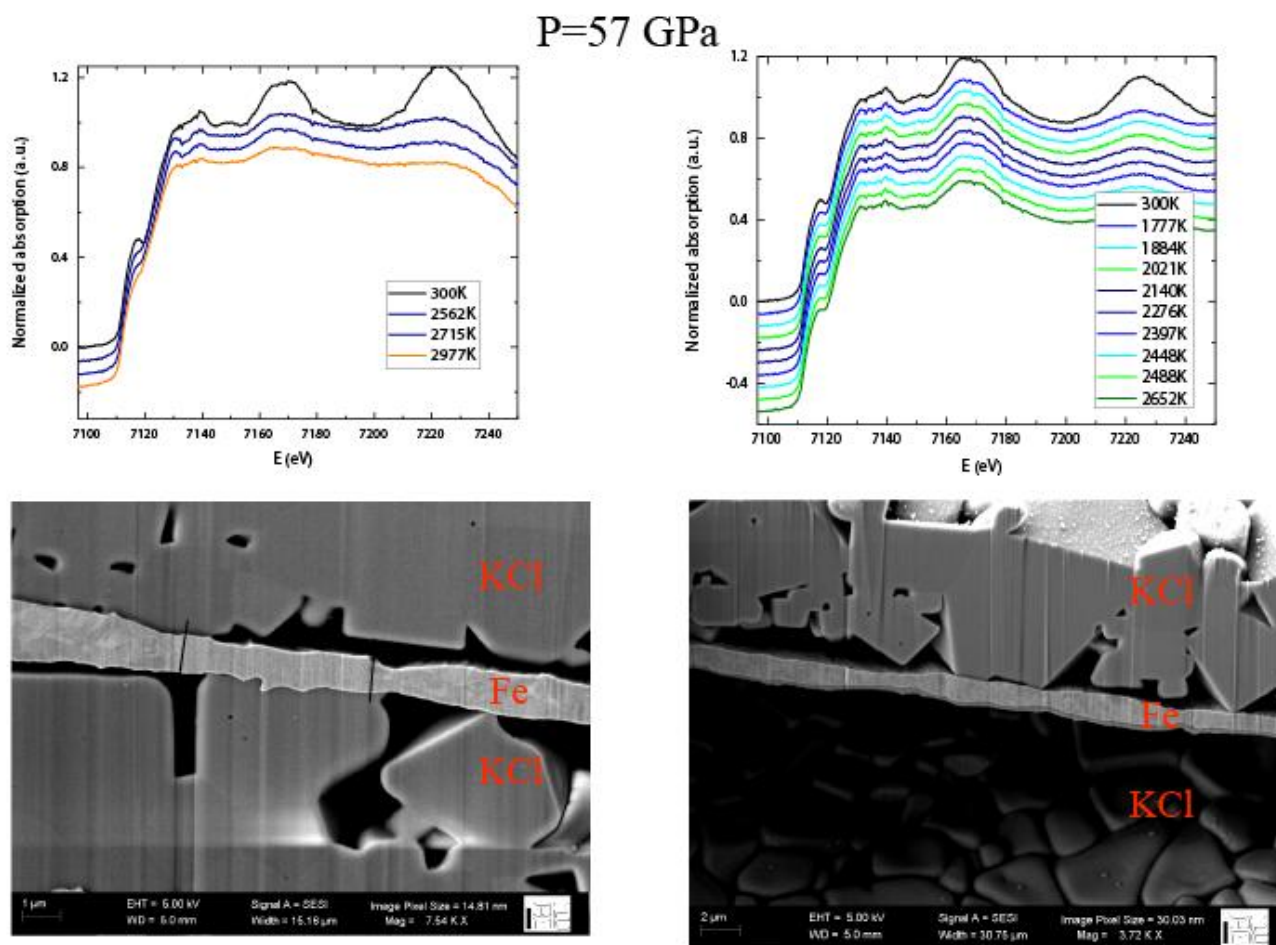


Figure 2: *Fe* XANES spectra changes as valid melting criteria. Series of XANES spectra as a function of increasing temperature above (left) and below (right) the melting temperature of *Fe*. This melting criterion has been validated by FIB cutting and SEM imaging of the hotspot cross section. Changes in the texture and irregular borders due to melting is identified on SEM figure on the left (The black lines delimitate the liquid portion of the sample). Full SEM images with a better resolution are available in the Supplementary Materials (Figure S5 and S6).

Along with the validation of the *in situ* melting criterion, a critical examination of the adopted metrology has been performed during the experiment. In particular, each temperature measurement has been analyzed via two-color pyrometry [Benedetti and Loubeyre, 2004] and individual error bars have been assigned (Figure S2). Concerning the pressure measurement, its value under high temperature is estimated considering the thermal contribution. In particular, the

value of this thermal pressure strongly depends on the pressure medium compressibility [Lord *et al.*, 2015], leading to small value when KCl is used: here, a constant value of 2 GPa has been assigned as based on XRD measurements of KCl embedded samples (see Methods section and Supplementary Materials). Individual error bars for pressure of ± 5 GPa is estimated to summarize the addition of different pressure uncertainties, such as pressure gradient in the sample chamber or uncertainty on the thermal pressure estimation for example.

Following the previous considerations, the melting points resulting from the SMS study [Jackson *et al.*, 2013; Zhang *et al.*, 2015], who used a sample geometry similar to the present one (Fe foil embedded in KCl), have been revised. In particular, the thermal pressure calculation presented here in the Supplementary Materials can be applied to the SMS studies [Jackson *et al.*, 2013; Zhang *et al.*, 2015], resulting in an excellent agreement between their recalculated melting temperatures, our XANES study and the previous XRD study of [Anzellini *et al.*, 2013] (Figure 3). The obtained results highlight the fact that these different *in situ* techniques are all valid and the previously observed differences arise from uncertainties in the metrology rather than on the adopted melting criteria. Therefore, a revised fit for the different phase boundary is presented to take into account small divergence (below 200 K) between XANES, SMS or XRD results, especially around the liquid-hcp-fcc triple point (Figure 3 and Supplementary Materials [Simon and Glatzel, 1929; Swartzendruber, 1982]).

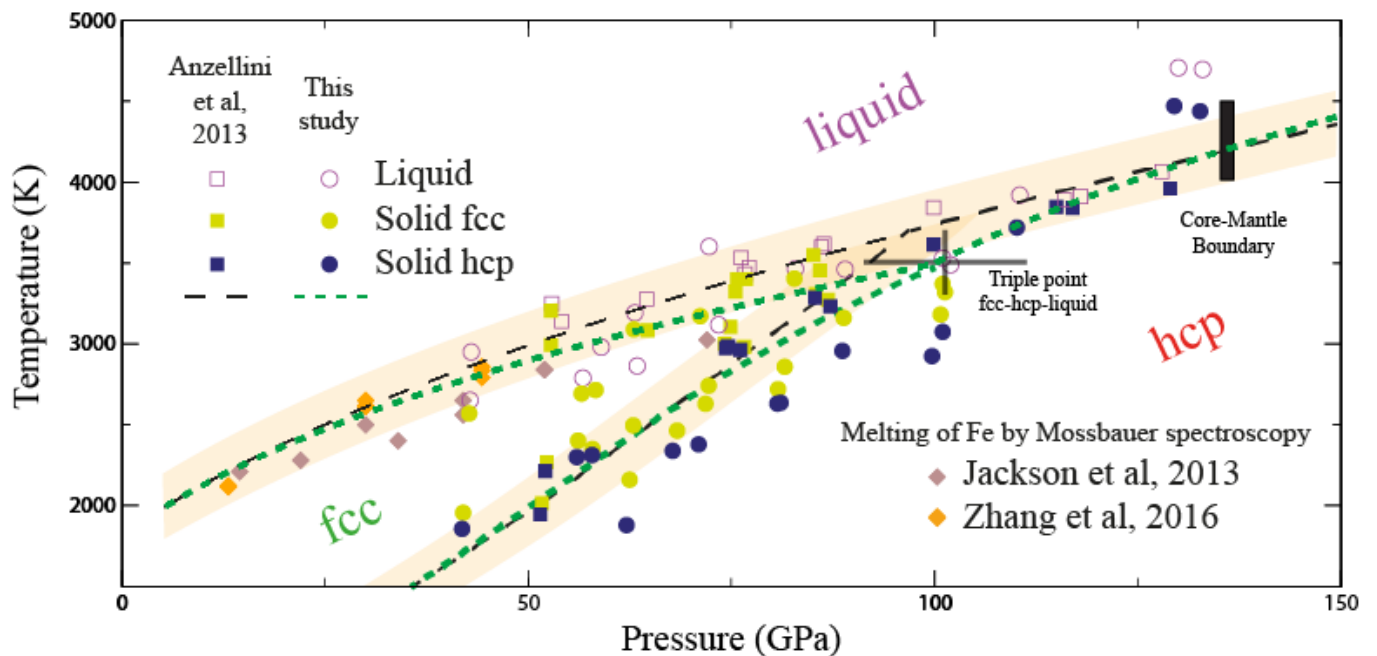


Figure 3: *Iron phase diagram combining our XANES dataset and previously published SMS and XRD dataset. Full squares and circles indicate the sample in the solid state for XRD [Anzellini et al., 2013] and XANES experiments respectively. Green color indicates the presence of fcc iron, and red color indicates the presence of hcp iron. Empty symbols indicate the presence of the first melt. Diamond symbols represent the melting of pure Fe measured by Synchrotron Mossbauer Spectroscopy [Jackson et al., 2013; Zhang et al., 2015], with thermal pressure rescaled following the present method (see Supplementary Materials for more information). The black dashed line represents the phase diagram boundaries from [Anzellini et al., 2013], whereas the green dashed line is adjusted to take into account the three different studies presented here (SMS, XRD and XANES studies) (Fitting parameters are available in the Supplementary Materials).*

The collected data allowed to bracket the melting curve of iron, between the last solid and the first appearance of the melt (**Figure 3; Table S1**). The measurements show an excellent agreement with the melting data from Anzellini et al (2013) from ambient pressure up to 80 GPa. A small discrepancy can be noticed around 80-100 GPa, where the present study supports a slight bending of the pure Fe melting curve around the hcp-fcc-liquid triple point. A flattening of the melting curve around the triple point can be expected, in relation to change in entropy of melting between the two solid polymorphs. A similar behavior is in fact observed in the case of Tin [Barnett et al., 1963]. According to our measurements, the triple point of pure Fe is located at 100 ± 10 GPa and 3500 ± 200 K.

Under higher pressures, our dataset follow a similar trend as Anzellini et al, (2013), however potentially showing higher melting temperature. But significant error bars on these two extreme pressure melting points (over 500 K) do not allow us to highlight a real divergence between the two studies at the CMB pressure. A melting temperature of 4250 ± 250 K is well representative of the present melting measurements.

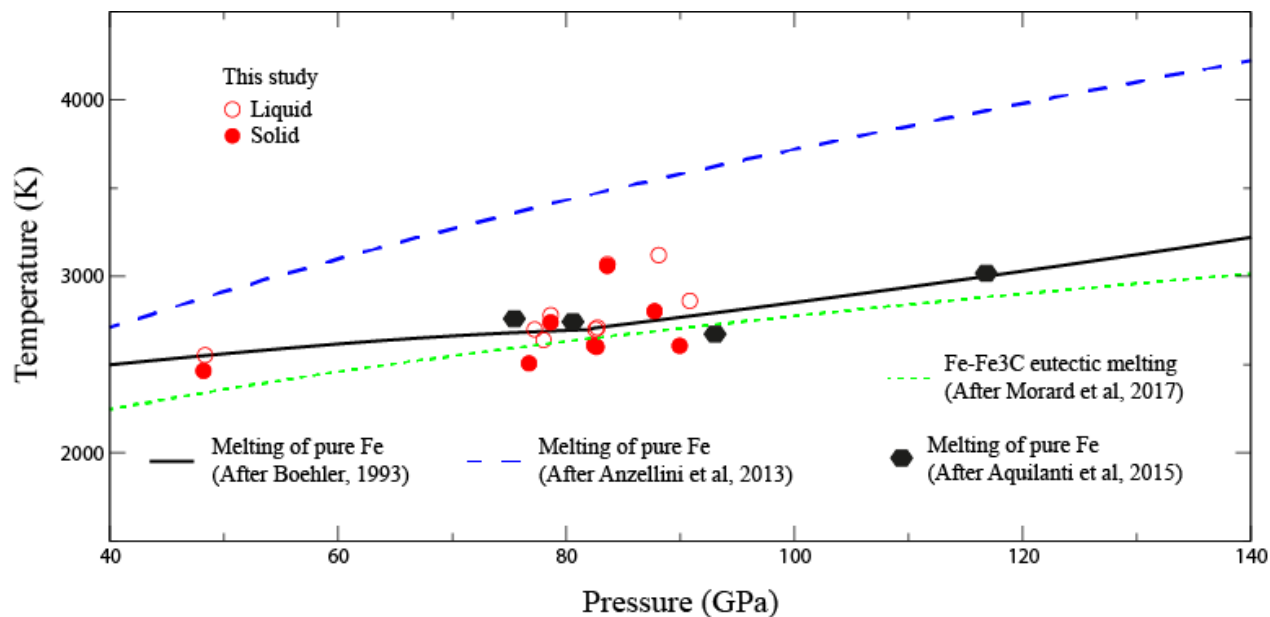


Figure 4: Melting curve of $Fe-Fe_3C$ compared with previous melting of pure Fe measurements and C contaminated samples from this study. Red circles represent last solid (full symbols) and first liquid (empty symbols) for melting measured by XANES in this study for carbon contaminated samples (see [Figure 1B](#)). These measurements are in good agreement with previous melting of Fe determination by speckle [Boehler, 1993] and by XANES [Aquilanti et al., 2015], highlighting that these studies may have determined melting of carbon contaminated Fe samples. For comparison, the eutectic melting in $Fe-Fe_3C$ system [Morard et al., 2017] is shown as green dashed line and pure Fe melting curve [Anzellini et al., 2013] is shown as blue dashed line.

In few laser-heating runs of the present study, significantly lower melting temperatures were obtained. Interestingly, these points agree with those reported in previous studies employing the XAS and/or speckle melting criterion [Boehler, 1993; Aquilanti et al., 2015] ([Figure 4](#)). For these samples, the melting signature on the Fe XANES is relatively similar to the highest temperature melting points ([Figure 5](#)). However, the signal of the quenched sample between each laser heating clearly highlights an evolution toward the disappearance of the pre-edge signal ([Figure 5](#)). We relate the lower sample melting temperatures to chemical reactions between the sample and the diamond anvils. Indeed, all low melting points are positioned relatively close to the $Fe-Fe_3C$ eutectic melting line [Lord et al., 2009; Morard et al., 2017]. In fact, the *ex situ* XRD analyses of recovered samples with low melting points show clearly the presence of Fe_3C diffraction peaks ([Figure 5](#)).

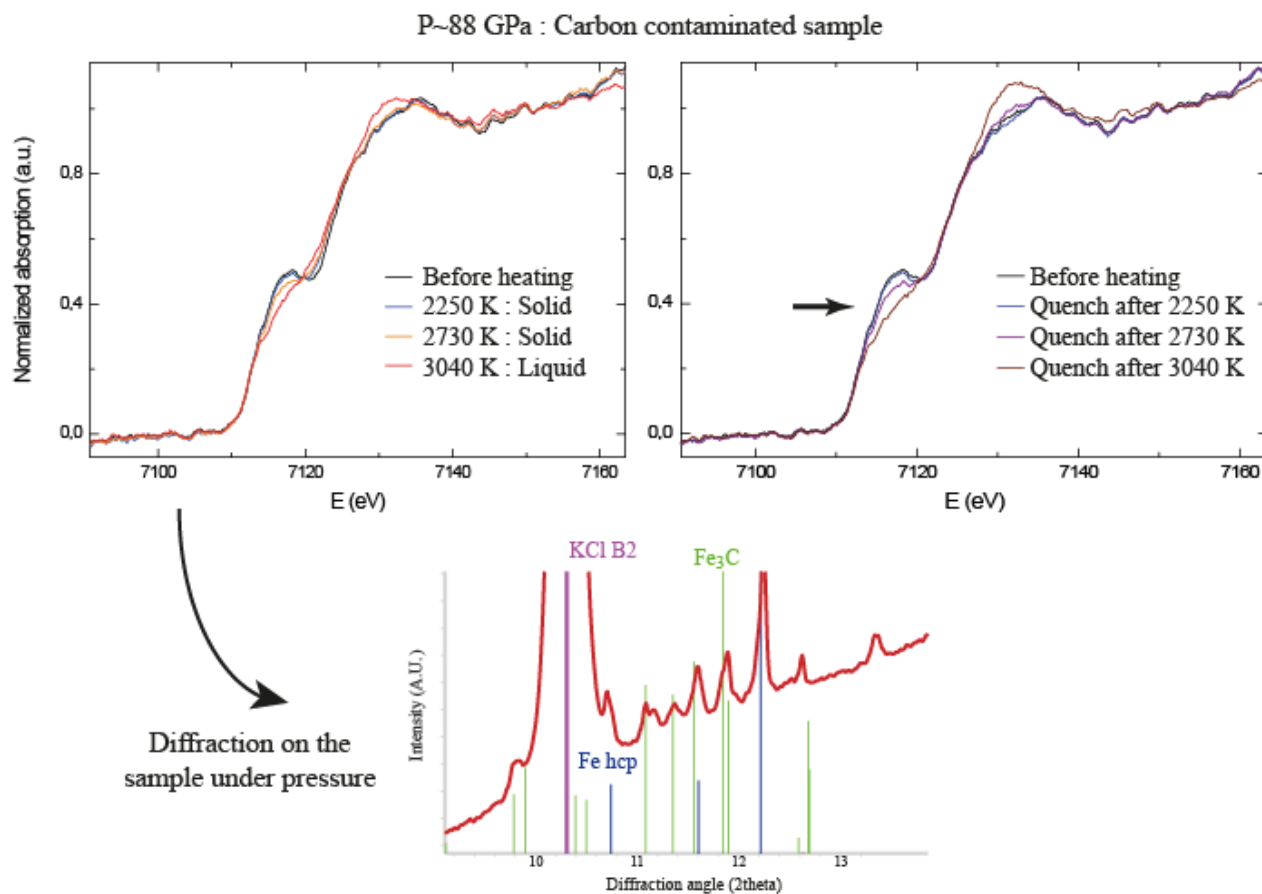


Figure 5: XANES spectra for carbon contaminated samples. Melting signature is relatively similar to the one for a pure Fe sample, whereas quench spectra clearly show an evolution related to the carbon enrichment (indicated by an arrow). In addition, diffraction on the sample kept under high pressure clearly shows diffraction peaks of Fe+Fe₃C mixture.

4. Discussion

The present experimental results highlight a convergence between the different experimental techniques used to probe melting in LH-DAC experiments. The melting criterion associated with changes in the XANES features has been validated through textural study of the recovered samples from high pressure laser-heating experiments. Probing the local environment of Fe atoms (XANES and SMS) gives the same melting temperature as probing longer-range structural change evidenced in XRD diffuse scattering appearance. The present critical record of sample reaction after each temperature step, and analysis of recovered samples, allowed us to evidence that lower melting temperatures are due to a carbon contamination of Fe sample. This

contamination is related to C migration through the pressure medium, reacting with iron in the solid state to form carbides, e.g. Fe₃C. This phenomenon has already been discussed in a previous study about carbon transport in LH-DAC [Prakapenka *et al.*, 2003].

We also demonstrate that the thermal pressure determination is an important origin of the observed discrepancies. Estimation of pressure at high temperatures is not straightforward for experiments where XRD signals under high temperature are not available *in-situ*. In the present study, the thermal pressure is estimated following XRD experiments with similar sample configuration, and it allowed us to reconcile SMS, XRD and XANES results. We would like to mention the recent attention on the careful comparison between reflective and refractive optics for temperature measurements [Mezouar *et al.*, 2017; Giampaoli *et al.*, 2018]. In the present data set an individual error bar is associated to each temperature measurement, using the sliding two-color analysis performed on a large range of wavelengths (from 650 to 900 nm⁻¹) (Figure S2). This allows to evaluate the robustness of the temperature for each individual X-ray acquisition.

Combining previous XRD and SMS dataset with the present XANES measurements allows to set the position of the triple point hcp-fcc-liquid in the iron phase diagram at 100 ± 10 GPa and 3500 ± 200 K. The location of this specific point is of first importance for the thermodynamic modeling of iron under high pressure [Komabayashi and Fei, 2010]. For example, the entropy change upon melting influencing the heat flow at the CMB could be derived from the position of the triple point [Anderson, 1990].

In addition, the melting temperature of pure Fe under CMB pressure is constrained at 4250 ± 250 K. This temperature is close to the solidus temperature of mantle materials (4180 K for peridotitic mantle [Fiquet *et al.*, 2010] and 4150 K for chondritic mantle [Andrault *et al.*, 2011]). However, the absence of extended silicate melting in contact with the metallic liquid outer core at the CMB implies that iron should be alloyed with light elements efficiently lowering its melting temperature. Therefore, volatile elements, such as sulfur, carbon or hydrogen [Mori *et al.*, 2016; Morard *et al.*, 2017], instead of silicon or oxygen, are required to significantly decrease the temperature of iron crystallization under Earth's core pressure.

5. Conclusions

Combined *in situ* XANES at Fe edge in LH-DAC and *ex situ* study of recovered samples by X-ray diffraction and microscopy analysis allowed an unambiguous determination of pure iron melting curve and phase diagram up to Core-Mantle Boundary pressure conditions. This dataset present an excellent agreement with previous *in situ* XRD [Anzellini *et al.*, 2013] and SMS [Jackson *et al.*, 2013], after recalculation of the thermal pressure estimation for the latest one. The triple point hcp-fcc-liquid in the iron phase diagram is estimated at 100 ± 10 GPa and 3500 ± 200 K and the melting temperature at CMB pressure (136 GPa) at 4250 ± 250 K. This melting temperature, relatively close to the melting temperature of mantle silicates at CMB pressure [Fiquet *et al.*, 2010; Andrault *et al.*, 2011], indicates that volatile light elements such as sulfur, carbon or hydrogen are required to lower the crystallization temperature of the Earth's liquid outer core and prevent extended melting of the mantle at the contact with the core.

Acknowledgments

Femtosecond laser micro-machining at the Institute de Minéralogie de Physique des Matériaux et de Cosmochimie (IMPMC), Paris has been developed and realized by the “Cellule Project” with the financial support of ANR 2010-JCJC-604-01.

Analysis of the recovered samples was performed with the help of I. Estève at the Focused Ion Beam (FIB) and Scanning Electron Microscope (SEM) facility of the Institute de Minéralogie de Physique des Matériaux et de Cosmochimie, supported by Région Ile de France grant SESAME 2006 N°I-07-593/R, INSU-CNRS, INP-CNRS, University Pierre et Marie Curie –Paris 6, and by the French National Research Agency (ANR) grant no. ANR-07-BLAN-0124-01.

This project has received funding from the European Research Council (ERC) under the European Union's Horizon 2020 research and innovation program (grant agreement No 670787).

Data are available as supporting information.

References

- Akahama, Y., and H. Kawamura (2004), High-pressure Raman spectroscopy of diamond anvils to 250 GPa: Method for pressure determination in the multimegabar pressure range, *J. Appl. Phys.*, *96*(7), 3748–3751, doi:10.1063/1.1778482.
- Alfè, D. (2009), Temperature of the inner-core boundary of the Earth: Melting of iron at high pressure from first-principles coexistence simulations, *Phys. Rev. B - Condens. Matter Mater. Phys.*, *79*(6), 1–4, doi:10.1103/PhysRevB.79.060101.
- Alfè, D., G. D. Price, and M. J. Gillan (2002), Iron under Earth's core conditions: Liquid-state thermodynamics and high-pressure melting curve from ab initio calculations, *Phys. Rev. B*, *65*(16), 165118, doi:10.1103/PhysRevB.65.165118.
- Anderson, O. L. (1990), The High-Pressure Triple Points of Iron and Their Effects On The Heat Flow From the Earth's Core, *J. Geophys. Res.*, *95*(B13), 21697–21707, doi:10.1029/JB095iB13p21697.
- Andrault, D., N. Bolfan-Casanova, G. Lo Nigro, M. A. Bouhifd, G. Garbarino, and M. Mezouar (2011), Solidus and liquidus profiles of chondritic mantle: Implication for melting of the Earth across its history, *Earth Planet. Sc. Lett.*, *304*(1–2), 251–259.
- Anzellini, S., A. Dewaele, M. Mezouar, P. Loubeyre, and G. Morard (2013), Melting of iron at earth's inner core boundary based on fast X-ray diffraction, *Science (80-.)*, *340*(6131), doi:10.1126/science.1233514.
- Aquilanti, G., A. Trapananti, A. Karandikar, I. Kantor, C. Marini, O. Mathon, S. Pascarelli, and R. Boehler (2015), Melting of iron determined by X-ray absorption spectroscopy to 100 GPa, *Proc. Natl. Acad. Sci.*, *112*(39), 12042–12045, doi:10.1073/pnas.1502363112.
- Barnett, J. D., R. B. Bennion, and H. T. Hall (1963), X-ray Diffraction Studies on Tin at High Pressure and High Temperature, *Science (80-.)*, *141*, 1041.
- Benedetti, L., and P. Loubeyre (2004), Temperature gradients, wavelength-dependent emissivity, and accuracy of high and very-high temperatures measured in the laser-heated diamond cell, *High Press. Res.*, *24*(4), 423–445, doi:10.1080/08957950412331331718.
- Boccatto, S., R. Torchio, I. Kantor, G. Morard, S. Anzellini, R. Giampaoli, R. Briggs, A. Smareglia, T. Irifune, and S. Pascarelli (2017), The Melting Curve of Nickel Up to 100 GPa Explored by XAS, *J. Geophys. Res. Solid Earth*, doi:10.1002/2017JB014807.
- Boehler, R. (1993), Temperatures in the Earth's core from melting-point measurements of iron at

- high static pressures, *Nature*, 363(6429), 534–536, doi:10.1038/363534a0.
- Boehler, R., D. Santamaría-Pérez, D. Errandonea, and M. Mezouar (2008), Melting, density, and anisotropy of iron at core conditions: New x-ray measurements to 150 GPa, *J. Phys. Conf. Ser.*, 121(PART 2), doi:10.1088/1742-6596/121/2/022018.
- Brown, J. M., and G. McQueen (1986), Phase Transitions , Griineisen Parameter , and Elasticity, *J. Geophys. Res.*, 91, 7485–7494.
- Campbell, A. J., L. Danielson, K. Righter, C. T. Seagle, Y. Wang, and V. B. Prakapenka (2009), High pressure effects on the iron-iron oxide and nickel-nickel oxide oxygen fugacity buffers, *Earth Planet. Sci. Lett.*, 286(3–4), 556–564, doi:10.1016/j.epsl.2009.07.022.
- Dewaele, A., M. Torrent, P. Loubeyre, and M. Mezouar (2008), Compression curves of transition metals in the Mbar range: Experiments and projector augmented-wave calculations, *Phys. Rev. B - Condens. Matter Mater. Phys.*, 78(10), 1–13, doi:10.1103/PhysRevB.78.104102.
- Fiquet, G., A. L. Auzende, J. Siebert, A. Corgne, H. Bureau, H. Ozawa, and G. Garbarino (2010), Melting of peridotite at 140 Gigapascals, *Science (80-.)*, 329, 1516–1518.
- Giampaoli, R., I. Kantor, M. Mezouar, S. Boccato, A. D. Rosa, R. Torchio, G. Garbarino, O. Mathon, and S. Pascarelli (2018), Measurement of temperature in the laser heated Diamond Anvil Cell: comparison between reflective and refractive optics., *High Press. Res.*, In press.
- Harmand, M. et al. (2015), X-ray absorption spectroscopy of iron at multimegabar pressures in laser shock experiments, *Phys. Rev. B - Condens. Matter Mater. Phys.*, 92(2), 1–7, doi:10.1103/PhysRevB.92.024108.
- Ishimatsu, N., K. Matsumoto, H. Maruyama, N. Kawamura, M. Mizumaki, H. Sumiya, and T. Irifune (2012), Glitch-free X-ray absorption spectrum under high pressure obtained using nano-polycrystalline diamond anvils, *J. Synchrotron Radiat.*, 19(5), 768–772, doi:10.1107/S0909049512026088.
- Jackson, J. M., W. Sturhahn, M. Lerche, J. Zhao, T. S. Toellner, E. E. Alp, S. V. Sinogeikin, J. D. Bass, C. A. Murphy, and J. K. Wicks (2013), Melting of compressed iron by monitoring atomic dynamics, *Earth Planet. Sci. Lett.*, 362, 143–150, doi:10.1016/j.epsl.2012.11.048.
- Kantor, I., C. Marini, O. Mathon, and S. Pascarelli (2018), A laser heating facility for energy-dispersive X-ray absorption spectroscopy, *Rev. Sci. Instrum.*, 89(1), 1–13, doi:10.1063/1.5010345.

- Komabayashi, T., and Y. Fei (2010), Internally consistent thermodynamic database for iron to the Earth's core conditions, *J. Geophys. Res. Solid Earth*, *115*(3), 1–12, doi:10.1029/2009JB006442.
- Lord, O. T., M. J. Walter, R. Dasgupta, D. Walker, and S. M. Clark (2009), Melting in the Fe-C system to 70 GPa, *Earth Planet. Sc. Lett.*, *284*(1–2), 157–167.
- Lord, O. T. et al. (2014), The NiSi melting curve to 70GPa, *Phys. Earth Planet. Inter.*, *233*, 13–23, doi:10.1016/j.pepi.2014.05.005.
- Lord, O. T., I. G. Wood, D. P. Dobson, L. Voigt, W. Wang, A. R. Thomson, E. T. H. Wann, G. Morard, M. Mezouar, and M. J. Walter (2015), The melting curve of Ni to 1 Mbar, *Earth Planet. Sci. Lett.*, *408*, 226–236, doi:10.1016/j.epsl.2014.09.046.
- Marini, C., F. Occelli, O. Mathon, R. Torchio, V. Recoules, S. Pascarelli, and P. Loubeyre (2014), A microsecond time resolved x-ray absorption near edge structure synchrotron study of phase transitions in Fe undergoing ramp heating at high pressure, *J. Appl. Phys.*, *115*(9), 1–5, doi:10.1063/1.4867619.
- Mazevet, S., V. Recoules, J. Bouchet, F. Guyot, M. Harmand, A. Ravasio, and A. Benuzzi-Mounaix (2014), Ab initio calculation of x-ray absorption of iron up to 3 Mbar and 8000 K, *Phys. Rev. B - Condens. Matter Mater. Phys.*, *89*(10), 1–5, doi:10.1103/PhysRevB.89.100103.
- Mezouar, M. et al. (2005), Development of a new state-of-the-art beamline optimized for monochromatic single-crystal and powder X-ray diffraction under extreme conditions at the ESRF, *J. Synchrotron Radiat.*, *12*(5), 659–664, doi:10.1107/S0909049505023216.
- Mezouar, M. et al. (2017), Methodology for in situ synchrotron X-ray studies in the laser-heated diamond anvil cell, *High Press. Res.*, *37*(2), 170–180, doi:10.1080/08957959.2017.1306626.
- Miozzi, F., G. Morard, D. Antonangeli, A. N. Clark, M. Mezouar, C. Dorn, A. Rozel, and F. G. (2018), Equation of state of SiC at extreme conditions: new insight into the interior of carbon rich exoplanets, *J. Geophys. Res. Planets*, *In press*.
- Morard, G. et al. (2017), Fe – FeO and Fe – Fe₃C melting relations at Earth's core – mantle boundary conditions : Implications for a volatile-rich or oxygen-rich core, *Earth Planet. Sci. Lett.*, *473*, 94–103, doi:10.1016/j.epsl.2017.05.024.
- Mori, Y., H. Ozawa, K. Hirose, R. Sinmyo, S. Tateno, G. Morard, and Y. Ohishi (2016), Melting

- experiments on Fe–Fe₃S system to 254 GPa, *Earth Planet. Sc. Lett.*, 464, Under Review, doi:10.1016/j.epsl.2017.02.021.
- Nguyen, J. H., and N. C. Holmes (2004), Melting of iron at the physical conditions of the Earth's core., *Nature*, 427(6972), 339–342, doi:10.1038/nature02248.
- Pascarelli, S., O. Mathon, T. Mairs, I. Kantor, G. Agostini, and C. Strohm (2016), The Time-resolved and Extreme-conditions XAS (TEXAS) facility at the European Synchrotron Radiation Facility : the energy-dispersive X-ray absorption spectroscopy beamline ID24, *J. Synchrotron Rad.*, 23, 353–368, doi:10.1107/S160057751501783X.
- Prakapenka, V., Shen, G., Dubrovinsky, L., 2003. Carbon transport in diamond anvil cells. *High Temp. Press.* 35/36, 237-249. doi:10.1068/htjr098
- Prescher, C., and V. B. Prakapenka (2015), DIOPTAS: A program for reduction of two-dimensional X-ray diffraction data and data exploration, *High Press. Res.*, 35(3), 223–230, doi:10.1080/08957959.2015.1059835.
- Simon, F., and G. Glatzel (1929), Bernerkungen zur Schmelzdruckkurve., *Z. Anorg. Allg. Chem.*, 178, 309.
- Swartzendruber, L. J. (1982), The Fe (Iron) System, *Bull. Alloy Phase Diagrams*, 3(2), 161–165.
- Torchio, R. et al. (2016), Probing local and electronic structure in Warm Dense Matter: Single pulse synchrotron x-ray absorption spectroscopy on shocked Fe, *Sci. Rep.*, 6(June), 1–8, doi:10.1038/srep26402.
- Zhang, D., J. M. Jackson, J. Zhao, W. Sturhahn, E. E. Alp, M. Y. Hu, T. S. Toellner, C. A. Murphy, and V. B. Prakapenka (2015), Temperature of Earth's core constrained from melting of Fe and Fe_{0.9}Ni_{0.1} at high pressures, *Earth Planet. Sci. Lett.*, 447, 72–83, doi:10.1016/j.epsl.2016.04.026.